Conformational Analysis of Chiral Ferrocene–Peptides

Katja Heinze,*[a] and Manuela Beckmann[a]

Dedicated to Professor Gottfried Huttner on the occasion of his 68th birthday

Keywords: Conformational analysis / Hydrogen bonds / Metallocenes / Modelling / Peptides

Ferrocene-containing dipeptides Ac-Fca-AA-OMe (AA = L-Val, L-Ile) with the artificial amino acid 1′-aminoferrocene-1-carboxylic acid (Fca) and chiral α-amino acid building blocks display hydrogen-bonded structures that result in organised helical ferrocene units in solution, as evidenced by spectroscopic and theoretical investigations.

Introduction

Short peptides usually exist as an ensemble of rapidly interconverting conformers in solution. However, intramolecular forces (hydrogen bonds, salt bridges, π-interactions) may stabilise a few preferred conformations even in small molecules.[1] In recent years, bioorganometallic chemistry has developed as a rapidly growing field, and this holds especially true for ferrocene as the organometallic ingredient.[2] The favourable electrochemical properties of ferrocenes have been exploited for use as redox probes in ferrocene-containing biomolecules. The almost unhindered rotational freedom of the ferrocene cyclopentadienyl rings might give rise to new structural and dynamic aspects in 1,1′-disubstituted ferrocene bioconjugates.[3]

We recently investigated the solid-state and solution structure of the *N*-protected active ester of 1′-aminoferrocene-1-carboxylic acid (Fca), benzotriazol-1-yl 1′-(acetylamino)ferrocene-1-carboxylate (Ac-Fca-OBt; Ac = acetyl, Bt = benzotriazol-1-yl) and found an intramolecular hydrogen bond both in the solid state and in solution with an activation barrier for the interconversion between enantiomeric conformations of 43 kJ mol^{-1}.[3] Kraatz et al. have reported the Boc-protected analogue and proposed a similar solution structure.[4]

Recently, Rapić and Metzler-Nolte reported the solid-state structure of the tetrapeptide Boc-Ala-Fca-Ala-Ala-OMe, which possesses two intramolecular hydrogen bonds that result in a (*P*)-helical arrangement of the Cp rings.[5] Similar observations on disubstituted ferrocene–peptide conjugates of ferrocenedicarboxylic acid have been reported by Hirao,[6,7] Kraatz[8] and Metzler-Nolte,[9] while the monosubstituted ferrocene–peptide conjugates of ferrocenecarboxylic acid frequently employed for labelling purposes do not exhibit a preferred helical arrangement at the ferrocene moiety.[6,7,9]

Simple chiral dipeptides of Fca, such as Ac-Fca-AA-OMe (AA = α-amino acid), possess just one chiral carbon atom in the vicinity of the ferrocene unit but should be able to display an intramolecular hydrogen bond which could result in a preferred conformation of the dipeptides in solution. Here we describe our results of a conformational analysis of Ac-Fca-AA-OMe (AA = L-Val, L-Ile) dipeptides in solution using spectroscopic and theoretical methods.

Results and Discussion

The dipeptides **1** and **2** were synthesised starting from the activated ester Ac-Fca-OBt[3] and H-Val-OMe·HCl and H-Ile-OMe·HCl, respectively (Scheme 1). The conjugates were fully characterised by mass spectrometry, showing the expected [M$^+$] peaks at m/z = 400 and 414, respectively, elemental analyses, IR spectroscopy (see Exp. Sect.) and cyclic voltammetry (oxidation waves at 535 and 565 mV vs. SCE, respectively).

In order to investigate the possible conformations of **1** and **2** in CH_2Cl_2 solution we performed NMR, IR and CD spectroscopic experiments with **1** and **2** in solution together with a theoretical analysis. The following discussion will at first focus on the conformations of **1** and subsequently a generalised conclusion will be attempted.

The ^{1}H NMR spectra of analytically pure samples of **1** in CD_2Cl_2 (Figure 1, Table 1) show two distinct species groups in the amide proton region and for the methyl group CH_3(A) in an approximate ratio of 10:1, which do not interconvert on the NMR timescale at 303 K {major con-

[a] Anorganisch-Chemisches Institut der Universität Heidelberg, Im Neuenheimer Feld 270, 69120 Heidelberg, Germany
Fax: +49-6221-545-707
E-mail: katja.heinze@urz.uni-heidelberg.de
Supporting information for this article is available on the WWW under http://www.eurjic.org or from the author.

  DOI: 10.1002/ejic.200500268

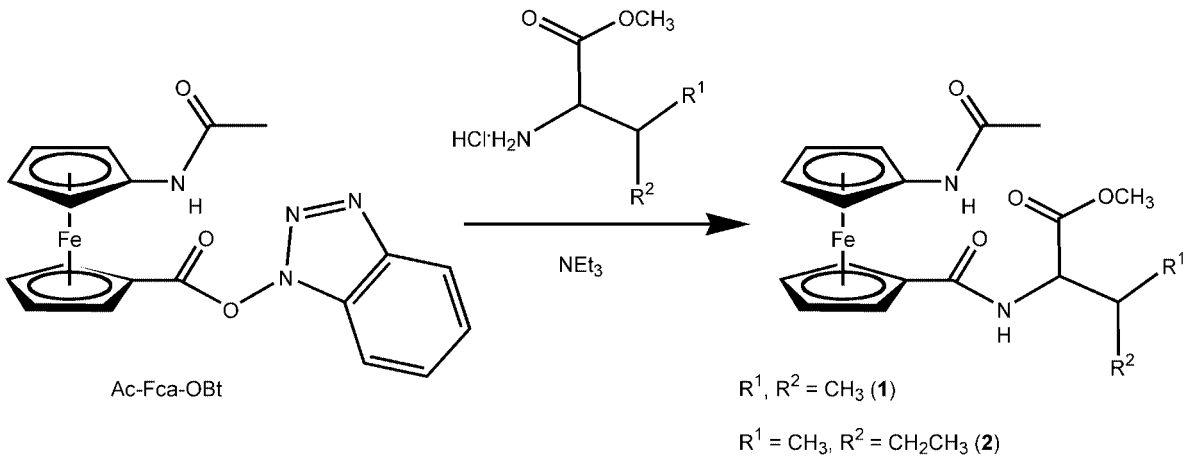

Scheme 1.

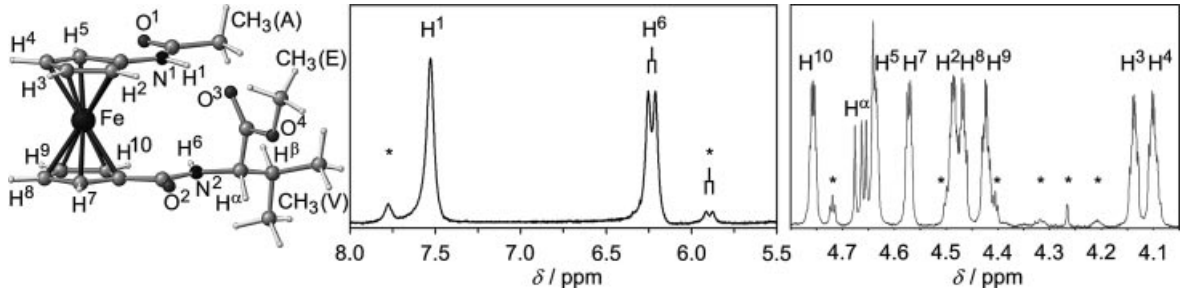

Figure 1. Left: atom numbering of **1**. ^{1}H NMR spectra of **1** in CD_2Cl_2 (10 mM); centre: amide region; right: Cp-H region (peaks labelled with an asterisk belong to minor conformations).

Table 1. ^{1}H NMR spectroscopic data of **1** and **2** (atom numbering according to Figure 1).

	1 (major)	**1** (minor)	**2** (major)	**2** (minor)
H^1	7.57 (m)	7.78 (s)	7.59 (m)	7.80 (s)
H^2/H^5	4.42 (m)/4.57 (m)		4.47 (m)/4.56 (m)	
H^3/H^4	4.04 (m)/4.07 (m)		4.03 (m)/4.07 (m)	
H^6	6.30 (d, 8.2 Hz)	5.84 (d, 8.0 Hz)	6.33 (d, 8.5 Hz)	5.7 (br)
H^7/H^{10}	4.51 (m)/4.69 (m)		4.50 (m)/4.69 (m)	
H^8/H^9	4.36 (m)/4.40 (m)		4.36 (m)/4.40 (m)	
H^α	4.59 (dvd, 8.8 Hz, 5.3 Hz)		4.63 (dvd, 8.5 Hz, 5.3 Hz)	
H^β	2.25 (dvqvq, 5.2 Hz, 7.0 Hz, 7.0 Hz)		1.97 (m)	
CH_3(A)	1.99 (s)	2.02 (s)	1.99 (s)	[a]
CH_3(E)	3.78 (s)		3.77 (s)	
CH_3(V)	0.97 (d, 7.2 Hz)		0.95 (pt, 7.4 Hz)	
CH_3(V)	0.99 (d, 7.2 Hz)		0.96 (d, 6.8 Hz)	
CH_2	–	–	1.26 (m), 1.50 (m)	

[a] Not observed due to overlap with H^β signal.

formers: $\delta(H^1)$ = 7.57 ppm, $\delta(H^6)$ = 6.30 ppm, $\delta[CH_3(A)]$ = 1.99 ppm; minor conformers: $\delta(H^1)$ = 7.78 ppm, $\delta(H^6)$ = 5.84 ppm, $\delta[CH_3(A)]$ = 2.02 ppm at 303 K}.

The cyclopentadienyl proton signals of the major conformers were assigned by 2D NMR experiments and a literature comparison[3,5,10] (Figure 1, Table 1). The expected NOE cross-peaks (intra-Cp, amide-Cp and within the L-valine unit) are observed in the NOESY spectra, while no cross-peaks are observed between the substituents. For the major species in CD_2Cl_2 solution all Cp protons are magnetically non-equivalent as the chiral carbon centre C^α of the L-amino acid part generates diastereotopic sides of the ferrocene both in the "lower" Cp ring (H^7/H^{10}: δ = 4.51/4.69 ppm; H^8/H^9: δ = 4.36/4.40 ppm) *and* in the "upper" Cp ring (H^2/H^5: δ = 4.42/4.57 ppm; H^3/H^4: δ = 4.04/4.07 ppm) which demonstrates that the chiral information is effectively transferred from the α-amino ester to the "lower" Cp *and* to the "upper" Cp ring. An analogous stereodiscrimination is found for the cyclopentadienyl carbon atoms (C^7/C^{10}: δ = 69.1/69.3 ppm; C^8/C^9: δ = 71.0/71.3 ppm; C^2/C^5: δ = 63.7/64.3 ppm; C^3/C^4: δ = 65.8/65.9 ppm).

Variable-temperature ^{1}H NMR spectra between 193 and 303 K allowed us to investigate the hydrogen-bonding situation of both conformer groups of **1** by monitoring the tem-

perature dependence of all amide proton signals. For the major conformers $\Delta\delta(H^1)$ = –6.8 ppb K^{-1} and $\Delta\delta(H^6)$ = –3.3 ppb K^{-1} (determined by a regression analysis between 243 and 303 K), thus showing that only H^1 is involved in a dynamic hydrogen bond, whereas for the minor conformers $\Delta\delta(H^1)$ = –5.9 ppb K^{-1} and $\Delta\delta(H^6)$ = –11.1 ppb K^{-1}, which suggests that *both* H^1 and H^6 are dynamically hydrogen-bonded [cf. non-hydrogen bonded Fc-NH-C(=O)-CH_3: $\Delta\delta(H^1)$ = –2.9 ppb K^{-1} and hydrogen-bonded Fc-NH-C(=O)-Fc-NH-C(=O)CH_3: $\Delta\delta(H^1)$ = –6.6 ppb K^{-1} and $\Delta\delta(H^6)$ = –11.0 ppb K^{-1}[3]].

The solution IR spectra of **1** (Figure 2) display signals due to hydrogen-bonded NH groups (3357 and 3325 cm^{-1}) together with free NH groups (3433 cm^{-1}), as well as absorption bands corresponding to hydrogen-bonded ester carbonyl groups (1728 cm^{-1}) and free ester groups (1739 cm^{-1}) in addition to several amide I (1664–1653 cm^{-1}) and amide II bands (1546–1512 cm^{-1}).

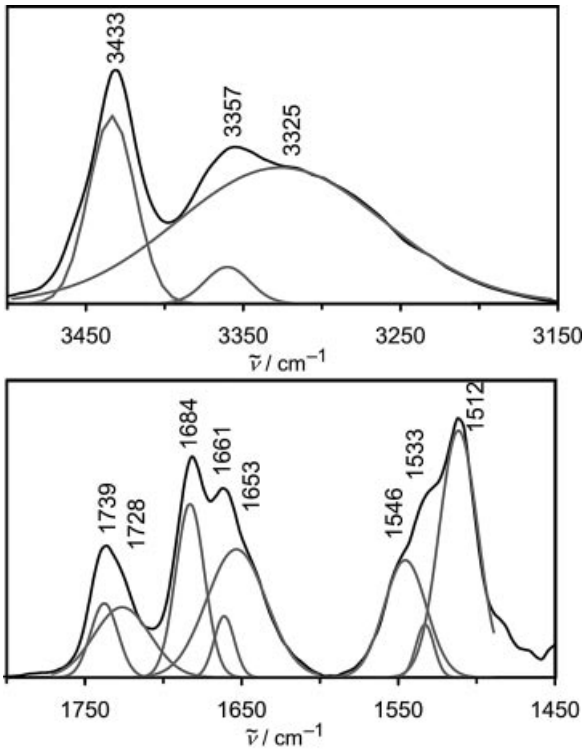

Figure 2. IR spectra of **1** in CH_2Cl_2 (left: amide A region; right: amide I+II region).

In the UV/Vis spectra the typical ferrocene absorption is observed at around 440 nm (see Exp. Sect.). The CD spectra of **1** and **2** in CH_2Cl_2 (Figure 3) display a positive Cotton effect at the ferrocene absorption (M_θ = 7440 and 6490 mdeg M^{-1} cm^{-1} at 450 nm for **1** and **2**, respectively) which is usually interpreted as a (*P*)-helical conformation of the ferrocene.[5,6,9] The CD signal intensity is diminished (M_θ = 3570 and 3210 mdeg M^{-1} cm^{-1} for **1** and **2**, respectively) by the addition of 20% (v/v) methanol, which might compete for hydrogen-bonding sites and result in a reduction of the helicity at the ferrocene. The negative CD at 500 nm might arise from minor conformations of **1** and **2** with (*M*)-helical ferrocene units or freely rotating Cp rings.[11]

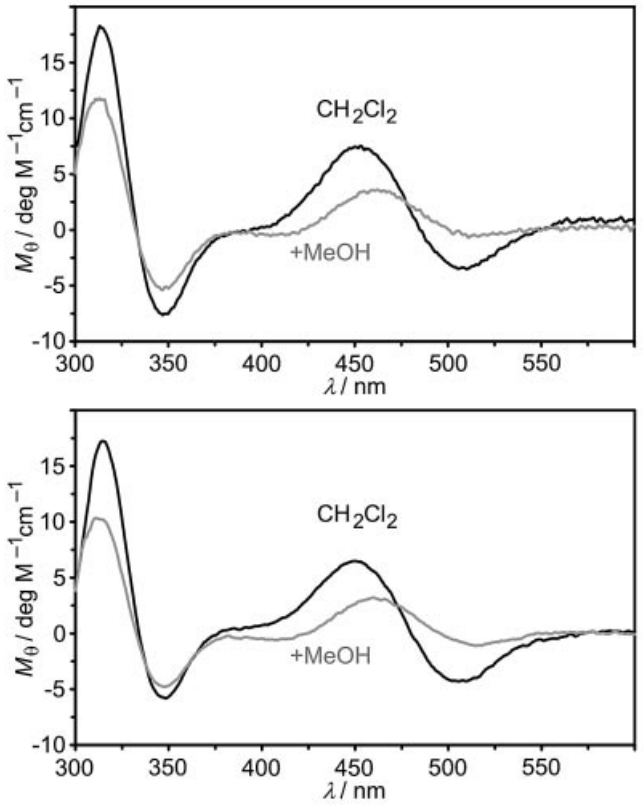

Figure 3. CD spectra of **1** (left) and **2** (right) (1 mM) in CH_2Cl_2 (dark line) and CH_2Cl_2/MeOH 20% (v/v) (light line).

Thus, ferrocene conjugates **1** and **2** appear to have similar helical conformations in CH_2Cl_2 solution that are destroyed in coordinating solvents. Additionally, NMR spectra in CD_2Cl_2/D_2O and CD_2Cl_2/DMSO/D_2O solvent mixtures reveal a different pattern in the Cp-H region between δ = 3.9 and 4.8 ppm, thus indicating different conformations in these solvent mixtures. In addition to the different pattern in the Cp-H region, the amide protons are exchanged against deuterium, with amide proton H^6 having a larger half-life than H^1, probably due the higher steric shielding of H^6 by the ester and alkyl groups of the α-amino acid part than for H^1.

A modelling study was performed in order to obtain more insight into the possible conformational space of the ferrocene–dipeptides. As force fields used in molecular mechanics calculations and dynamics simulations are currently not available for ferrocene derivatives, we employed the DFT method. DFT calculations (B3LYP, LanL2DZ) on **1** in the gas phase with varying starting geometries resulted in an ensemble of ten stable hydrogen-bonded conformations (Figure 4, Table 2), which fall into four categories (**RL**, **LR**, **LL** and **RR**) that differ in the relative orientation of the NH vectors (R and L denote a clockwise and anticlockwise rotation, respectively, of the N^1H^1 and N^2H^6 vectors when looking along the [centroid C^1–C^5]–[centroid C^6–C^{10}] axis). Different types of intramolecular hydrogen bonds (**a**:

$H^1\cdots O^3$; **b**: $H^1\cdots O^2$; **c**: $H^6\cdots O^1$) are observed within these groups. No minimum structure could be found for conformers **RL-c** and **LR-c** with the NH vectors directed towards each other and with a hydrogen bond between H^6 and O^1 as the geometry optimisations always converge to structures **RL-b** and **LR-b**, respectively. In fact, **RL-c** rather corresponds to the transition state of the isomerisation **RL-a** → **LL-c** (Table 2). Likewise, the non-hydrogen-bonded geometries **RL-d**, **LL-d** and **RR-d** represent transition states with one imaginary frequency for the Cp ring rotation rather than minimum structures, while **LR-d** again represents a local minimum (Figure 5, Table 2).

The relative energies of the different conformations fall into a narrow region of 0–30 kJ mol^{-1} as expected for a small peptide (Table 2). In spite of these small energy differences, an attempt to explain the experimental data on the basis of the calculated geometries and energies was undertaken. From the conformer population data it is reasonable to include only conformers **RL-a**, **RL-b**, **LR-b**, **LL-a**, **LL-b** and **LL-c** in the following interpretation of the experimental data (Figure 4, highlighted structures; see also Table 2 and Scheme 2).

The observation of hydrogen-bonded ester carbonyl groups (type **a** hydrogen bond: **RL-a** and **LL-a**) together

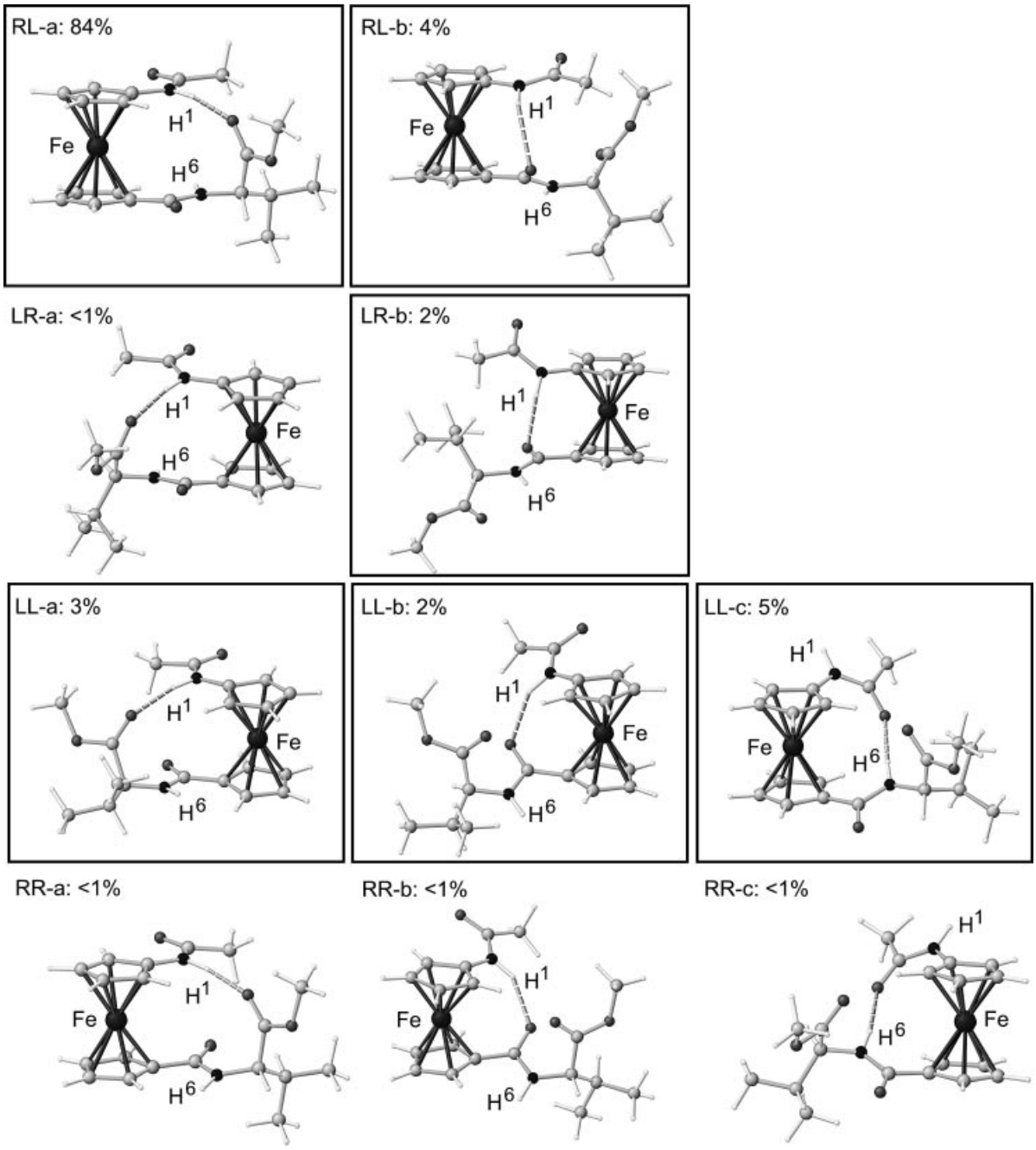

Figure 4. Ensemble of DFT-calculated hydrogen-bonded minimum structures of **1** with the major conformations highlighted.

Table 2. Energetic and geometric parameters calculated for the conformers of **1** by DFT methods (B3LYP, LanL2DZ).

Conformer	Relative energy [kJ mol^{-1}]	Conformer population [%][a]	α [°][b]	Hydrogen bond [Å]
RL-a	0	83.9	+46.4	$H^1\cdots O^3$ = 1.92
RL-b	7.5	4.1	–7.2	$H^1\cdots O^2$ = 2.44
LR-a	19.6	<1	–38.9	$H^1\cdots O^3$ = 1.92
LR-b	9.1	2.1	+4.7	$H^1\cdots O^2$ = 2.04
LL-a	8.3	2.9	–32.0	$H^1\cdots O^3$ = 1.94
LL-b	9.3	2.0	–48.4	$H^1\cdots O^2$ = 2.01
LL-c	7.0	5.0	+84.2	$H^6\cdots O^1$ = 1.91
RR-a	20.9	<1	+27.2	$H^1\cdots O^3$ = 1.95
RR-b	26.7	<1	+48.3	$H^1\cdots O^2$ = 2.02
RR-c	21.9	<1	–82.1	$H^6\cdots O^1$ = 1.83
RL-d	24.9[c]	–	–177.8	–
LR-d	12.1[d]	<1	+149.9	–
LL-d	21.8[e]	–	+166.4	–
RR-d	23.4[f]	–	–179.3	–
RL-a → LL-c	24.6[g]	–	+38.5	$H^6\cdots O^1$ = 2.25 ($H^1\cdots O^3$ = 3.43)
LL-a → LL-b	16.2[h] (7.9[i])	–	–42.1	($H^1\cdots O^3$ = 3.04) $H^1\cdots O^2$ = 2.39

[a] Conformer populations were calculated by using a Boltzmann distribution at 298 K. [b] The torsion angle, α, is defined as C^1–[centroid C^1–C^5]–[centroid C^6–C^{10}]–C^6. [c] This geometry corresponds to a transition state with N_{imag} = 1 (16.7i cm^{-1}; Cp ring rotation). [d] This geometry corresponds to a minimum (N_{imag} = 0). [e] This geometry corresponds to a transition state with N_{imag} = 1 (5.5i cm^{-1}; Cp ring rotation). [f] This geometry corresponds to a transition state with N_{imag} = 1 (11.0i cm^{-1}; Cp ring rotation). [g] This geometry corresponds to a transition state with N_{imag} = 1 (45.7i cm^{-1}; combined Cp ring rotation, *N*-acetyl rotation and hydrogen-bond breaking). [h] This geometry corresponds to a transition state with N_{imag} = 1 (32.6i cm^{-1}; combined Cp ring rotation and hydrogen-bond breaking). [i] Energy relative to **LL-a**.

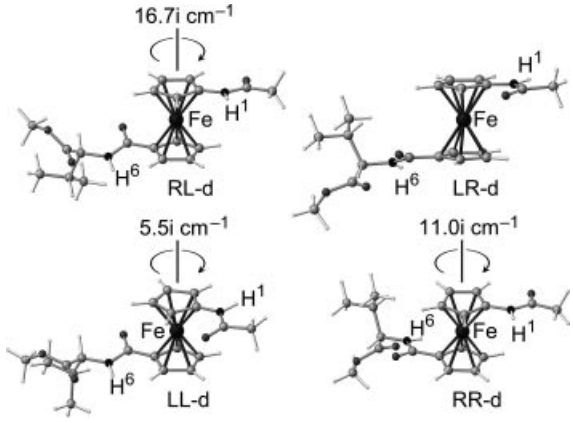

Figure 5. Non-hydrogen bonded structures of **1**.

with free ester carbonyl groups, as well as hydrogen-bonded amide carbonyl groups (type **b** and **c** hydrogen bonds: **RL-b**, **LR-b**, **LL-b**, **LL-c**) together with free amide carbonyl groups, in the calculated conformers is in agreement with the experimental IR spectroscopic data (Figures 2 and 4).

On the basis of their relative abundance, the two signal sets with relative intensity of 91% and 9% observed in the ^{1}H NMR spectra are assigned to groups **RL** (calculated conformer population 88%) and **LL** (calculated conformer population 10%), respectively, while populations of group **LR** and group **RR** fall below the detection limit of NMR spectroscopy.

Interconversion within the NMR-observable conformer groups **RL** and **LL** is fast on the NMR timescale as only time-averaged NMR signals are observed for each group (Scheme 2). Thus, the activation barrier for the involved processes hydrogen-bond breaking and Cp-ring rotation should be rather small. The activation barriers for these elementary steps can be estimated to be 8 kJ mol^{-1} for hydrogen-bond breaking and 5–10 kJ mol^{-1} for Cp-ring rotation[12] (13–18 kJ mol^{-1} for both steps; cf. energies of non-hydrogen-bonded species **d** in Table 2). In fact, a transition state for the conformational rearrangement **LL-a** → **LL-b** could be located only 7.9 kJ mol^{-1} above **LL-a**.

However, for the transformation **RL** → **LL**, in addition to hydrogen-bond breaking and Cp-ring rotation, the *N*-acetyl group has to flip relative to the Cp plane, which results in an additional activation barrier of 17–25 kJ mol^{-1} [rotational barrier estimated for the model compound (acetylamino)ferrocene Ac–NH–Fc; Figure 6[13]]. Thus, in total the energy required for this stepwise pathway **RL-a** → **RL-d** → *N*-acetyl rotation → **LL-d** → **LL-a**/**LL-b**/**LL-c** can be estimated to lie in the range 30–43 kJ mol^{-1}. For **RL-a** → **LL-c** a direct low-energy hydrogen-bond-assisted pathway combining *N*-acetyl rotation and Cp-ring rotation could be found with a transition state 24.6 kJ mol^{-1} higher in energy than **RL-a** (Figure 7, Scheme 2). Even the energy for this direct pathway is substantially higher than that estimated for the easy transformation between **a**, **b** and **c** conformers. Thus, the DFT calculations provide a qualitative rationale for the observation of two slowly interconverting species groups (Scheme 2).

The assignment of the major conformers to group **RL** and the minor conformers to group **LL** was further supported by the variable-temperature ^{1}H NMR spectra as the major conformers only possess $H^1\cdots$O hydrogen bonds (**RL-a**, **RL-b**) while the minor conformers have $H^1\cdots$O *and* $H^6\cdots$O hydrogen bonds (**LL-a**, **LL-b** and **LL-c**, Figure 4, Scheme 2) in agreement with the observed large temperature dependence of the signal for proton H^6 in the minor species group.

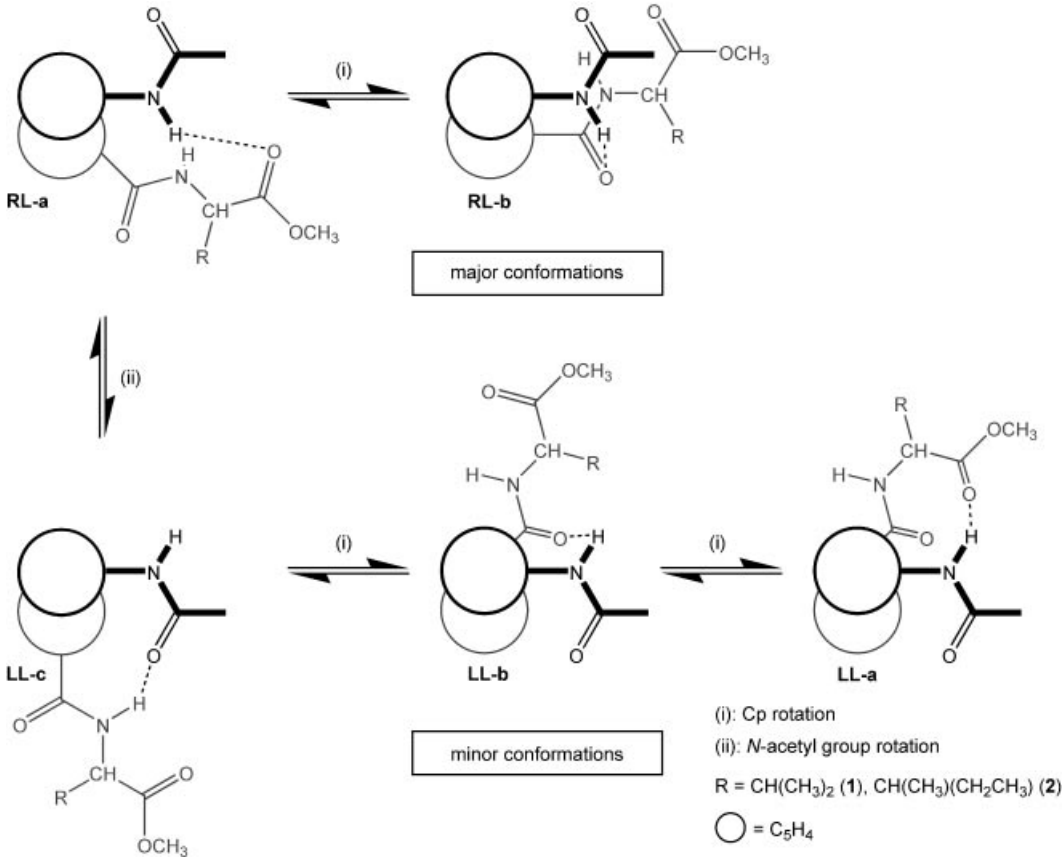

Scheme 2.

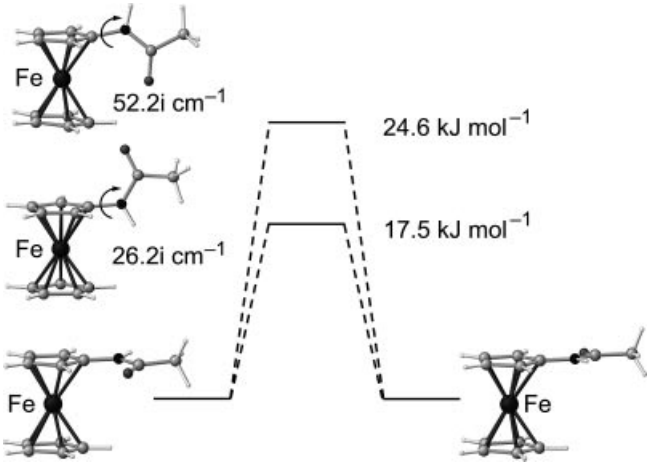

Figure 6. Energy profile for the *N*-acetyl group rotation in the model complex Ac-NH-Fc.

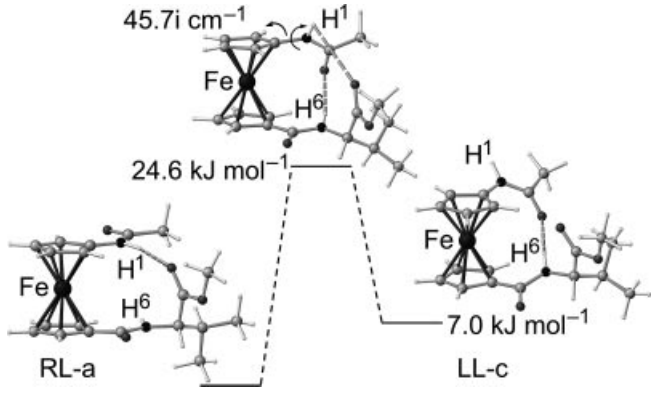

Figure 7. Energy profile for the hydrogen-bond-assisted direct conversion **RL-a** → **LL-c**.

Due to the restrained relative orientation of the ferrocene chromophore and the chiral centre due to the hydrogen bonding the ferrocene itself gains helical chirality, which results in fairly large Cotton effects compared to those of monosubstituted ferrocenes with a chiral centre in the substituent.[11] The dominant (*P*)-helical conformation of the ferrocene unit suggested by the CD spectra (Figure 3) can be explained by conformers **RL-a**, **LR-b** and **LL-c** with positive torsion angles *a*, which together amount to 91% of the species according to the calculations (Table 2). Thus, the DFT modelling of the conformational space of **1**, albeit not in a strictly quantitative sense, can explain all the experimental findings (IR, NMR and CD data).

For the isoleucine derivative **2** the experimental data are almost identical to those of **1** (see Exp. Sect. and Supporting Information), thereby suggesting a similar conformation of **2** in solution. Figure 8 depicts the calculated minimum structure of **2** (analogous to **RL-a** with a population of 62%; see Supporting Information), which has a Cp torsion angle, *a*, of +47.3°. This observation points to the fact

that a second chiral carbon centre (C^{β}) in the side-chain of the isoleucine moiety has only a marginal influence on the ferrocene conformation and that the preferred ferrocene helicity in these dipeptides is determined by the configuration of the C^{α} atom of the α-amino acid.

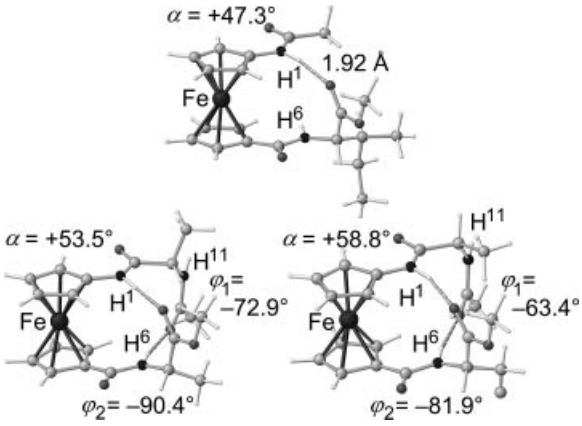

Figure 8. DFT calculated minimum structure of **2** (top), Ac-Ala-Fca-Ala-OMe (bottom left) and Ac-D-Ala-Fca-Ala-OMe (bottom right) [φ_1 and φ_2 are the C(=O)–C^{α}–N–C(=O) torsion angles].

To further corroborate the above interpretations the tripeptides Ac-Ala-Fca-Ala-OMe and Ac-D-Ala-Fca-Ala-OMe, which possess two intramolecular hydrogen bonds, were modelled (Figure 8) and the ferrocene helicity and amide backbone torsion angles φ [C(=O)-N–C^{α}-C(=O)] compared to those of the structurally characterised tetrapeptide Boc-Ala-Fca-Ala-Ala-OMe.[5] For the tetrapeptide, values of $\alpha = +60.7°$, $\varphi_1 = -81.3°$ and $\varphi_2 = -90.1°$ have been determined in the solid state, and these compare well with the calculated values for the tripeptide Ac-Ala-Fca-Ala-OMe ($\alpha = +53.5°$, $\varphi_1 = -72.9°$ and $\varphi_2 = -90.4°$), further supporting the above interpretations. This finding suggests that the ferrocene helicity is determined by the configuration of the first C-terminal amino acid rather than the configuration of the N-terminal amino acid. In fact, replacing the N-terminal L-Ala by D-Ala results in a very similar conformation (Ac-D-Ala-Fca-Ala-OMe: $\alpha = +58.8°$, $\varphi_1 = -63.4°$ and $\varphi_2 = -81.9°$; Figure 8).

Conclusions

One chiral carbon atom within the C-terminal substituent at the organometallic amino acid Fca is sufficient to induce helical chirality at the ferrocene provided that an efficient hydrogen-bonding pathway exists between the two cyclopentadienyl rings. The conformer **RL-a**, which accounts for the major conformation of **1** and **2** in solution, possesses a (*P*)-helical ferrocene unit. The helicity is induced by a single intramolecular amide-to-ester hydrogen bond as the chirality-transfer pathway. The organised chiral secondary structures of small Fca-containing peptides open up an opportunity to design selective receptors[14–17] and homodisperse oligomers[13a,18] with well-defined secondary structures containing neutral or cationic ferrocene units in the backbone. Further work in these directions is currently in progress.

Experimental Section

General: Unless noted otherwise, all manipulations were carried out under argon by means of standard Schlenk techniques. All solvents were dried by standard methods and distilled under argon prior to use. All other reagents were used as received from commercial sources. NMR: Bruker Avance DPX 200 at 200.15 MHz and Varian Unity Plus 400 at 399.89 MHz (^{1}H); chemical shifts (δ) in ppm with respect to residual solvent peaks as internal standard: CD_2Cl_2 (^{1}H: δ = 5.32 ppm). IR spectra were recorded with a BioRad Excalibur FTS 3000 spectrometer using CaF_2 cells in CH_2Cl_2. Cyclic voltammetry was performed using an EG&G model 273 potentiostat, a glassy carbon electrode, a platinum electrode and an SCE electrode, 10^{-3} M in 0.1 M nBu$_4$NBF$_4$/CH_2Cl_2; potentials are given relative to that of SCE; $E_{1/2}$ of the Fc/Fc$^+$ couple under the experimental conditions is 420(10) mV vs. SCE. Circular dichroism spectra were recorded with a JASCO J-810 spectropolarimeter in 1-cm Suprasil cells thermostatted at 20 °C under argon. Mass spectra were recorded with a Finnigan MAT 8400 spectrometer with 4-nitrobenzyl alcohol as the matrix (FAB). Elemental analyses were performed by the microanalytical laboratory of the Organic Chemistry Department, University of Heidelberg. Melting points were determined with a Gallenkamp capillary melting point apparatus MFB 595 010 and are uncorrected.

Computational Methods: Density functional calculations were carried out with the Gaussian03/DFT[19] series of programs. The B3LYP formulation of density functional theory was used with the LanL2DZ basis set.[19] Geometry optimisations were performed using the Berny algorithm as implemented in Gaussian03. Convergence criteria were as follows: maximum force 0.00045; root-mean-square of forces 0.0003; maximum displacement 0.0018; root-mean-square displacements 0.0012. All points were characterised as minima ($N_{imag} = 0$) or first-order saddle points ($N_{imag} = 1$) by frequency analysis.

Synthesis of 1 and 2: A solution of the activated ester Ac-Fca-OBt in THF was treated with 1 equiv. of H-Val-OMe·HCl (for **1**) or H-Ile-OMe·HCl (for **2**) and 1 equiv. of NEt_3 and stirred at ambient temperature for 3 h. The solvent was then removed under reduced pressure and the residue was dissolved in dichloromethane. The solution was washed with water, aqueous $NaHCO_3$, saturated NaCl and 2% citric acid. The organic layer was dried with $MgSO_4$ and the solvent was removed under reduced pressure to give an orange powder. **1:** Yield: 160 mg, 0.40 mmol (82%). $C_{19}H_{24}FeN_2O_4$ (400.26): calcd. C 57.02, H 6.04, N 7.00; found C 57.20, H 6.09, N 7.18. UV/Vis (CH_2Cl_2): λ = 441 nm (270 M^{-1}cm^{-1}). ^{13}C{^{1}H} NMR (CD_2Cl_2): δ = 173.1 (C=O$_{ester}$), 169.8 (C=O$_{acetyl}$), 168.7 (C=O$_{amide}$), 94.6 (Cp-C_q), 76.5 (Cp-C_q), 71.3, 71.0 (C^8, C^9), 69.3, 69.1 (C^7, C^{10}), 65.9, 65.8 (C^3, C^4), 64.3 (C^2), 63.7 (C^5), 57.2 (C^{α}), 52.1 [CH_3(E)], 31.2 (C^{β}), 23.9 [CH_3(A)], 19.4, 18.3 [CH_3(V)] ppm. MS (FAB): *m/z* (%) = 400 (95) [M$^+$]. IR (CsI): $\tilde{\nu}$ = 3290 (NH), 3094, 2966, 2935 2874, 2857 (CH), 1745 (CO$_{ester}$), 1668, 1636 (amide I), 1560, 1539 (amide II) cm^{-1}. M.p. 66 °C. **2:** Yield: 194 mg, 0.46 mmol (78%). $C_{20}H_{26}FeN_2O_4$ (414.28): calcd. C 57.98, H 6.33, N 6.76; found C 57.96, H 6.32, N 7.40. UV/Vis (CH_2Cl_2): λ = 438 nm (300 M^{-1}cm^{-1}) ppm. ^{13}C{^{1}H} NMR (CD_2Cl_2): δ = 173.1 (C=O$_{ester}$), 169.8 (C=O$_{acetyl}$), 168.8 (C=O$_{amide}$), 94.7 (Cp-C_q), 76.5 (Cp-C_q), 71.3, 71.0 (C^8, C^9), 69.3, 69.2 (C^7, C^{10}), 65.9, 65.8 (C^3, C^4), 64.3 (C^2), 63.7 (C^5), 56.5 (C^{α}), 52.1 [CH_3(E)], 37.1 (C^{β}), 25.1 (CH_2), 23.2 [CH_3(A)], 15.3 [CH_3(V)], 11.0 (CH_2CH_3) ppm. MS (EI): *m/z* (%)

= 414 (100) [M^+]. IR (CsI): $\tilde{\nu}$ = 3298 (NH), 3091, 2965, 2934 2878, 2856 (CH), 1746 (CO_{ester}), 1670, 1636 (amide I), 1562, 1542 (amide II) cm^{-1}. IR (CH_2Cl_2): $\tilde{\nu}$ = 3431, 3355, 3325 (sh) (NH), 1735 (CO_{ester}), 1682, 1660, 1654 (sh) (amide I), 1550 (s), 1533 (sh), 1512 (amide II) cm^{-1}. M.p. 68 °C.

Supporting Information (see footnote on the first page of this article): Coordinates of all minimum structures and transition states, a table of energetic and geometric parameters calculated for the conformers of **2** by DFT methods (B3LYP, LanL2DZ) and IR spectra of **1** and **2** in CH_2Cl_2.

Acknowledgments

This work was supported by the Deutsche Forschungsgemeinschaft, the Fonds der Chemischen Industrie and the Dr. Otto Röhm Gedächtnisstiftung. The generous support of Prof. Dr. G. Huttner is gratefully acknowledged. We thank Prof. Dr. N. Metzler-Nolte for valuable discussions and for giving us access to the CD spectropolarimeter.

[1] N. Sewald, H.-D. Jakubke, *Peptides: Chemistry and Biology*, Wiley-VCH **2002**.
[2] D. N. van Staveren, N. Metzler-Nolte, *Chem. Rev.* **2004**, *104*, 5931–5985.
[3] K. Heinze, M. Schlenker, *Eur. J. Inorg. Chem.* **2004**, 2974–2988.
[4] K. A. Mahmoud, Y.-T. Long, G. Schatte, H.-B. Kraatz, *Eur. J. Inorg. Chem.* **2005**, 173–180.
[5] L. Barišić, M. Dropucic, V. Rapić, H. Pritzkow, S. I. Kirin, N. Metzler-Nolte, *Chem. Commun.* **2004**, 2004–2005.
[6] T. Moriuchi, A. Nomoto, K. Yoshida, T. Hirao, *Organometallics* **2001**, *20*, 1008–1013.
[7] T. Moriuchi, A. Nomoto, K. Yoshida, A. Ogawa, T. Hirao, *J. Am. Chem. Soc.* **2001**, *123*, 68–75.
[8] F. E. Appoh, T. C. Sutherland, H.-B. Kraatz, *J. Organomet. Chem.* **2004**, *689*, 4669–4677.
[9] X. de Hatten, T. Weyhermüller, N. Metzler-Nolte, *J. Organomet. Chem.* **2004**, *689*, 4856–4867.
[10] H.-B. Kraatz, J. Lusztyk, G. D. Enright, *Inorg. Chem.* **1997**, *36*, 2400–2405.
[11] Amino acid conjugates of ferrocenecarboxylic acid Fc-CO-NH-CHR-COOEt show weak, positive Cotton effects at 450 nm and stronger, negative Cotton effects at 500 nm. For R = $CH_2CH(CH_3)_2$: M_θ = 50 mdeg M^{-1} cm^{-1} (450 nm) and M_θ = –100 mdeg M^{-1} cm^{-1} (500 nm): H. Falk, C. Krasa, K. Schlögl, *Monatsh. Chem.* **1969**, *100*, 1552–1563. For R = $CH_2CH_2SCH_3$: M_θ = 402 mdeg M^{-1} cm^{-1} (460 nm) and M_θ = –1610 mdeg M^{-1} cm^{-1} (500 nm): Ref.[9]
[12] The experimental rotational barrier of unsubstituted ferrocene has been determined to be 1–5 kJ mol^{-1}: a) L. N. Mulay, A. Atalla, *J. Am. Chem. Soc.* **1963**, *85*, 702–706; b) A. Haaland, J. E. Nilsson, *J. Chem. Soc., Chem. Commun.* **1968**, *2*, 88–89; c) S. Sorriso, G. Cardaci, S. M. Murgia, *J. Organomet. Chem.* **1972**, *44*, 181–184; d) A. B. Gardner, J. Howard, T. C. Waddington, R. M. Richardson, J. Tomkinson, *Chem. Phys.* **1981**, *57*, 453–460. The rotational barrier calculated for ferrocene by DFT is 6.0 kJ mol^{-1} (44.6i cm^{-1}), which is in good agreement with the experiment. The barrier calculated for Ac-NH-Fc by DFT is 7.1 kJ mol^{-1} (16.9i cm^{-1}). See Supporting Information.
[13] The barrier for the N-ring rotation in acetanilide has been recently calculated as 18 kJ mol^{-1}, which is in very good agreement with the low-energy barrier calculated for Ac-NH-Fc: a) R. J. Doerksen, B. Chen, D. Liu, G. N. Twe, W. F. DeGrado, M. L. Klein, *Chem. Eur. J.* **2004**, *10*, 5008–5016; b) W. Caminati, A. Maris, A. Millemaggi, *New J. Chem.* **2000**, *24*, 821–824. The amide-plane rotation barrier calculated for Fc-CO-NH_2 is higher (estimated 35–40 kJ mol^{-1}) due to the onset of double-bond localisation: L. Lin, A. Berces, H.-B. Kraatz, *J. Organomet. Chem.* **1998**, *556*, 11–20.
[14] K. Heinze, M. Schlenker, *Eur. J. Inorg. Chem.* **2005**, 66–71.
[15] P. D. Beer, *Acc. Chem. Res.* **1998**, *31*, 71–80.
[16] P. D. Beer, P. A. Gale, *Angew. Chem.* **2001**, *113*, 502–532; *Angew. Chem. Int. Ed.* **2001**, *40*, 486–516.
[17] T. Schrader, A. D. Hamilton, *Functional Synthetic Receptors*, Wiley-VCH **2005**.
[18] a) J. S. Nowick, M. Pairish, I. Q. Lee, D. L. Holmes, J. W. Ziller, *J. Am. Chem. Soc.* **1997**, *119*, 5413–5424; b) H. Q. Zeng, R. S. Miller, R. A. Flowers, B. Gong, *J. Am. Chem. Soc.* **2000**, *122*, 2635–2644; c) J. T. Ernst, J. Becceril, H. S. Park, H. Yin, A. D. Hamilton, *Angew. Chem.* **2003**, *115*, 553–557; *Angew. Chem. Int. Ed.* **2003**, *42*, 535–539; d) D. Liu, S. Choi, B. Chen, R. J. Doerksen, D. J. Clements, J. D. Winkler, M. L. Klein, W. F. DeGrado, *Angew. Chem.* **2004**, *116*, 1178–1182; *Angew. Chem. Int. Ed.* **2004**, *43*, 1158–1162.
[19] M. J. Frisch, G. W. Trucks, H. B. Schlegel, G. E. Scuseria, M. A. Robb, J. R. Cheeseman, J. A. Montgomery, Jr., T. Vreven, K. N. Kudin, J. C. Burant, J. M. Millam, S. S. Iyengar, J. Tomasi, V. Barone, B. Mennucci, M. Cossi, G. Scalmani, N. Rega, G. A. Petersson, H. Nakatsuji, M. Hada, M. Ehara, K. Toyota, R. Fukuda, J. Hasegawa, M. Ishida, T. Nakajima, Y. Honda, O. Kitao, H. Nakai, M. Klene, X. Li, J. E. Knox, H. P. Hratchian, J. B. Cross, C. Adamo, J. Jaramillo, R. Gomperts, R. E. Stratmann, O. Yazyev, A. J. Austin, R. Cammi, C. Pomelli, J. W. Ochterski, P. Y. Ayala, K. Morokuma, G. A. Voth, P. Salvador, J. J. Dannenberg, V. G. Zakrzewski, S. Dapprich, A. D. Daniels, M. C. Strain, O. Farkas, D. K. Malick, A. D. Rabuck, K. Raghavachari, J. B. Foresman, J. V. Ortiz, Q. Cui, A. G. Baboul, S. Clifford, J. Cioslowski, B. B. Stefanov, G. Liu, A. Liashenko, P. Piskorz, I. Komaromi, R. L. Martin, D. J. Fox, T. Keith, M. A. Al-Laham, C. Y. Peng, A. Nanayakkara, M. Challacombe, P. M. W. Gill, B. Johnson, W. Chen, M. W. Wong, C. Gonzalez, J. A. Pople, *Gaussian 03*, revision B.03, Gaussian, Inc., Pittsburgh, PA, USA, **2003**.

Received: March 29, 2005
Published Online: August 1, 2005

